



A unified seakeeping and manoeuvring model with a PID controller for path following of a KVLCC2 tanker in regular waves

Paramesh S., Suresh Rajendran*

Department of Ocean Engineering, IIT Madras 600036, India



ARTICLE INFO

Keywords:

Unified seakeeping and manoeuvring model
PID controller
KVLCC2
Line of sight(LOS)

ABSTRACT

Heading control of ships in calm water has been investigated by several authors using different control techniques. However, the study on heading control of ships in actual sea conditions is very limited. This paper attempts to investigate the heading control in regular waves using a PID controller. A 6 DoF unified seakeeping and manoeuvring numerical model is integrated with a PID controller. A crude oil carrier (KVLCC2) prototype is used in the numerical study. The second order wave mean drift forces are calculated based on Salvesen's method and affect the horizontal motions. The wave exciting forces/moments and the restoring forces in the vertical planes are calculated for the exact wetted surface area. Empirical relations available in the existing literature are used to compute the propeller thrust, control forces/moments and hydrodynamic forces. PID controller gains K_p , K_d and K_i changes for different sea states depending on the external wave force. Hence these gains are pre-calculated for different sea states by trial and error. The performance of the controller under the wave action is then studied for path-following application.

1. Introduction

Traditionally, the manoeuvring and seakeeping characteristics of ships are analysed separately. This is due to the fact that the manoeuvring is important inside port and harbour where only limited space is available for the vessel to manoeuvre. Inside these sheltered areas, the ship encounters waves of insignificant wave height. Hence the manoeuvring simulations are traditionally conducted in calm water. Moreover, seakeeping and manoeuvring are problems of different time scales and hence treated separately, i.e., manoeuvring is a low frequency problem while seakeeping is a high frequency problem. However, due to the recent International Maritime Organization (IMO) regulations on the ship's energy efficiency, manoeuvring in waves has also become an important topic of concern among the industrial and research community. The slow steaming of ships (introduced as an effort to reduce the emission) can reduce the manoeuvring capability of ships in waves because of the additional wave forces and ineffectiveness of rudder due to slow ship speed. A unified model will facilitate safe ship manoeuvring in waves. In this paper, a unified seakeeping and manoeuvring model integrated with an autopilot is proposed for practical engineering applications. During manoeuvring in waves, the high frequency wave forces affect the low frequency manoeuvring forces through the second order drift forces. To the best knowledge of the authors, only a very few studies have been conducted on the integration of an autopilot in an unified seakeeping and manoeuvring

model in order to study the path following characteristics of a vessel moving in moderate to extreme sea condition. The unified model helps to calculate the wave forces that are accurate for practical engineering applications and hence reduce the uncertainty in the system modelling.

Several kinds of research have been conducted on the manoeuvring of ships in calm water. Son and Nomoto (1981), Yoshimura (2001), Xiang and Faltinsen (2011), Yasukawa and Yoshimura (2015), Sutulo and Soares (2019) conducted numerical studies and Skjetne et al. (2004), Moreira and Soares (2011), Perera et al. (2012), Kim et al. (2019) conducted experimental studies on ship manoeuvring in calm water. Bailey (1997) developed unified seakeeping and manoeuvring mathematical model based on linear convolution integral to describe ship's behaviour in irregular waves. However, the presence of convolution integral requires higher computational time than a frequency dependent solution. Researchers have proposed various approximation methods that reduce the computational time required to compute the convolution integral present in the Cummins formulation (Jefferys, 1984; Paul, 1998; Duclos et al., 2001). Ottosson and Bystrom (1991), Fossen (2005) and Fang et al. (2005) presented non-linear time domain models that do not take into account wave memory effects and thus avoided convolution integral. Sutulo and Guedes Soares (2008) followed a similar approach to estimating the hydrodynamic loads acting on manoeuvring ships in regular waves in the time domain. Fonseca and Guedes Soares

* Corresponding author.

E-mail address: sureshr@iitm.ac.in (S. Rajendran).

(1998), Fonseca (1998) and Rajendran et al. (2015b) demonstrated the importance of considering the time varying wetted surface area of the hull in evaluating wave induced vertical motions and loads on ships. The authors considered the body non-linearity associated with the time varying wetted surface of the hull while estimating the hydrostatic and Froude-Krylov forces in a seakeeping problem. Skejic and Faltinsen (2008) studied the wave effects on ship manoeuvring using a 4 DoF model based on a two time scale approach. The authors investigated the influence of incident waves on manoeuvring predictions through mean 2nd order wave loads. Yasukawa and Nakayama (2009), Yen et al. (2010) and Seo and Kim (2011) also followed a two time scale approach with the mean 2nd order wave loads for the manoeuvring predictions in waves. Yasukawa and Yoshimura (2015) predicted the manoeuvring motions of a KVLCC2 tanker in calm water using MMG standard method. This method laid out a standard procedure to capture ship's hydrodynamic characteristics, analysed them to determine the hydrodynamic coefficients and predicted the manoeuvring motions. Manoeuvring performance of ships in seaway was also carried out by using CFD technique based on finite volume method (Peric and Bertram, 2011; Bertram, 2011), Boundary element method (BEM), etc. However, the application of CFD technique in real time simulations is limited due to its higher computational resource and time requirement. Kim et al. (2019) presented the experimental results for turning circle characteristics of KVLCC2 tanker in regular waves for different sea conditions and analysed them in terms of drifting distance and drift angle.

Conventional PID controllers may not perform as expected in changing environmental conditions. In recent decades, various control techniques have been proposed to improve the controller performance in changing environmental conditions. Moradi and Katebi (2001) used linear models for the controller design in ship autopilots. The author used a general predictive algorithm to calculate the optimal gains for PID controller. Lee et al. (2009) studied the ship's motion control in shallow waters and deep waters using PID control algorithm and fuzzy logic control algorithm. Tomera (2017) used the fuzzy self-tuning method to auto-tune the PID controller gains. The proposed control algorithm's performance was shown to be improved in terms of settling time and the overshoot both numerically and experimentally. Trajectory tracking of under-actuated surface vessels has been studied by Pettersen and Nijmeijer (1998), Jiang and Nijmeijer (1999), Sira-Ramirez (1999) and Do et al. (2002). The models proposed by these authors try to achieve simultaneous control in all 3 degrees of freedom (x , y , ψ) using two control inputs and these models are not robust to environmental disturbances. Conventional methods in their simplest form achieve path following by controlling a single state, i.e., ψ (Lekkas and Fossen, 2013; Fossen et al., 2003; Oh and Sun, 2010; Tran, 2014). Guerreiro et al. (2014) applied a model based control technique, non-linear model predictive control (NMPC), for trajectory tracking of the autonomous surface craft. The author considered the state constraints in the form of penalties in the cost function. The input constraints are made inherent in the non-linear model to reduce the computational burden. The proposed algorithm is also tested for real-time implementation on a catamaran model. Zheng et al. (2014) compared the performance of Nonlinear Model Predictive Control (NMPC) and Linearized Model Predictive Control (LMPC) techniques for trajectory tracking of surface vessels in calm water in terms of computational facility required for the optimization of the quadratic objective function, accuracy and the efficiency of the two methods. Fossen et al. (2014) developed an adaptive controller to compensate for the drift due to the environmental disturbance in the path following problem. Several other authors have developed different control techniques to improve the performance as well as to compensate for the environmental disturbances (Encarnacao and Pascoal, 2000; Wang et al., 2018; Xu et al., 2020). Though there are several advanced control techniques available in the literature, the PID control technique is still widely implemented in industrial applications because of its feasibility and ease of implementation in real-time.

Table 1
Turning circle parameters.

Particular	No. of segments	Time step Δt	Advance	Tactical dia.	Transfer
20	0.05	3.05	3.10	1.8	
		0.1	3.08	3.10	1.8
		0.15	3.08	3.10	1.78
Numerical	40	0.05	3.16	3.11	1.82
		0.1	3.18	3.11	1.8
		0.15	3.18	3.11	1.8
60	0.05	3.18	3.11	1.82	
		0.1	3.18	3.13	1.8
		0.15	3.18	3.13	1.8

Generally, in a ship path following controller problem, the wave drift forces and the corresponding drift angle, aka side slip angle, are considered as unknowns which leads to uncertainty in the system modelling. Instead of that, the accuracy of a PID controller based autopilot system in regular waves is investigated in this paper through a unified seakeeping and manoeuvring numerical tool. Manoeuvring part of the model is based on the MMG model. In this model, separate modules are modelled for propeller, rudder and hull forces. The hydrodynamic derivatives, propeller and rudder characteristics were calculated experimentally by Yasukawa and Yoshimura (2015) for the KVLCC2 tanker. To reduce uncertainty in the estimation of the hydrodynamic derivative during turning, the Circular Motion Test (CMT) was used instead of Planar Motion Mechanism (PMM). Yasukawa and Yoshimura (2015) used these hydrodynamic derivatives in a 3DoF equation of motion and the turning circle trajectory was numerically simulated. The numerical turning circle characteristics (like diameter, transfer and advance) were compared with their experimental results and the error was found to be less than 5%. Therefore, these hydrodynamic derivatives are used in our paper for investigating the path following characteristics of the tanker. The wave forces are calculated based on well known 'strip theory' approximation. Here the ship is approximated as a slender body, which is a valid assumption because the L/B ratio is greater than 5. The wave force modelling is based on the potential flow method because the viscosity is not important unless the wave breaking happens. In our study, we are testing the ship in moderate seas. Therefore the potential theory is a valid assumption. Hence the controller's design based on an unified model helps in modelling the autopilot system and the controller gains that are accurate enough for practical engineering applications and are applicable for different sea states prior to the sailing of the ship.

The second order wave drift forces affects the manoeuvring performance and are considered in the surge, sway and yaw degrees of freedom. The first order wave exciting forces are calculated for each time instant based on the exact position of the hull which gives a good approximation of the body non-linear wave forces (Rajendran et al., 2015b). These high frequency forces are considered for the heave, roll and pitch motions. The resulting ordinary differential equations are solved in the time domain using Runge-Kutta 4th order numerical method with constant time step. In the first part of this paper, the numerical results are compared with the experimental results for open-loop turning circle tests in calm water and waves. In the second part of this paper, a PID controller is integrated with the 6 DoF model for heading control in regular waves. The PID controller gains are found for different wave conditions and the performance of the controller is investigated using path following in these wave conditions.

2. Unified numerical model

Rajendran et al. (2015b, 2016) presented a body non-linear time domain method based on strip theory for sea-keeping calculation. The

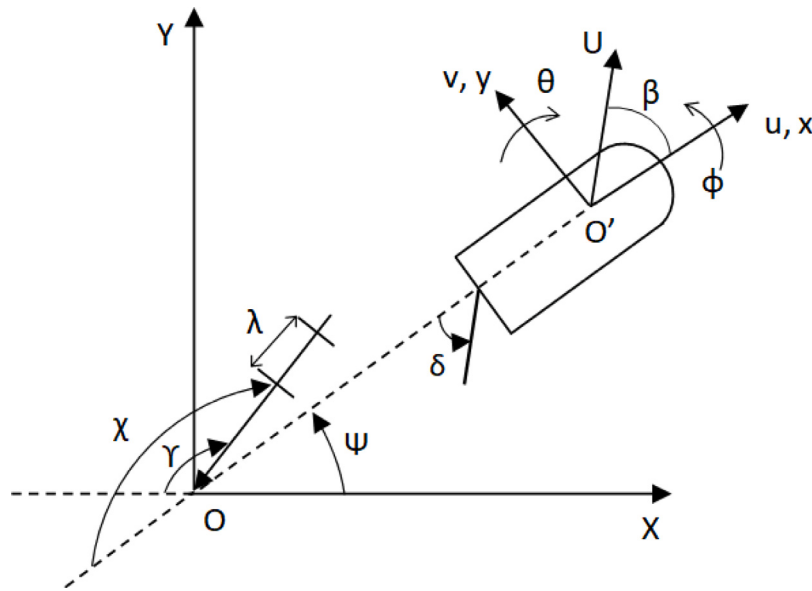


Fig. 1. Coordinate systems and conventions followed for manoeuvring simulations.

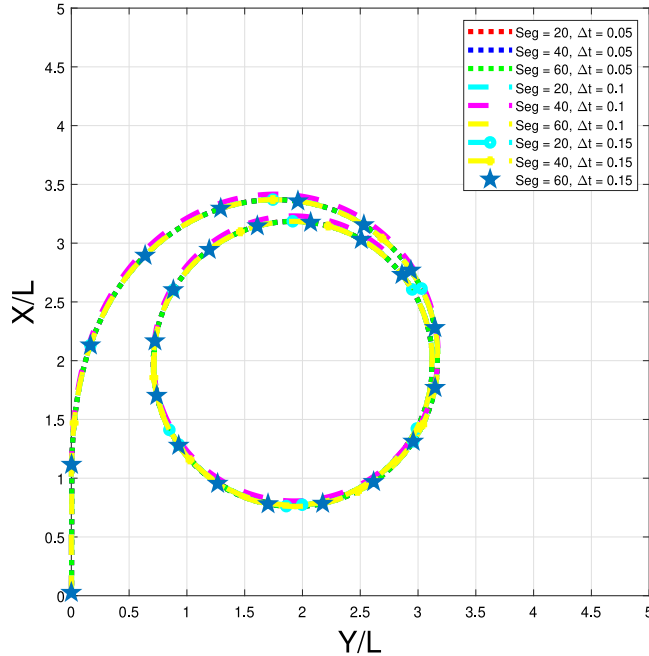


Fig. 2. Numerical solution with different number of segments and time step.

numerical tool is further modified to study the manoeuvring performance of ships. A 6 DoF model in the body frame is given by the expression below,

$$\dot{\eta} = R(\eta)v$$

$$[M + A]\ddot{v} + B_{RB}v + Cv = F_P + F_R + F_H + F_{Rest} + (F_{FK} + F_D)_i + (F_{Secondorderdrift})_j \quad (1)$$

where $i, j = 1, 2, \dots, 6$, $(F_{FK} + F_D)_{i=1,2,6} = 0$ and $(F_{Secondorderdrift})_{j=3,4,5} = 0$

A right handed co-ordinate system is followed as shown in Fig. 1. The manoeuvring problem is solved in the body frame, xyz , that is fixed at amidship and coincides with the mean water level. The positive z axis is pointing upwards and the positive yaw motion is anti-clockwise. Similarly, a right-handed coordinate system XYZ is followed for the

inertial frame. Both the inertial and body frames coincide with each other at the starting of the simulation. The waves are represented in the inertial frame and are coming at an incident angle of γ w.r.t earth fixed frame as shown in Fig. 1. $\gamma = 180^\circ$ is considered as the head sea condition. The wave encounter heading angle, i.e., with respect to the body frame, is $\chi = \psi + \gamma$.

The ship is assumed to have lateral symmetry and that the centre of gravity is located at $(x_c, 0, z_c)$. The mass matrix (M) is given by,

$$M = \begin{bmatrix} M & 0 & 0 & 0 & Mz_c & 0 \\ 0 & M & 0 & -Mz_c & 0 & Mx_c \\ 0 & 0 & M & 0 & -Mx_c & 0 \\ 0 & -Mz_c & 0 & I_x & 0 & -I_{xz} \\ Mz_c & 0 & -Mx_c & 0 & I_y & 0 \\ 0 & Mx_c & 0 & -I_{xz} & 0 & I_z \end{bmatrix} \quad (2)$$

and the Coriolis component matrix due to rigid mass is given by,

$$B_{RB} = \begin{bmatrix} 0 & -Mr & Mq & 0 & 0 & 0 \\ Mr & 0 & -Mp & 0 & 0 & 0 \\ -Mq & Mp & 0 & 0 & 0 & 0 \\ 0 & 0 & 0 & 0 & -I_{xz}q + I_zr & -I_yq \\ 0 & 0 & 0 & -I_zr + I_{xz}p & 0 & I_{xz}r + I_xp \\ 0 & 0 & 0 & I_yq & I_{xz}r - I_xp & 0 \end{bmatrix} \quad (3)$$

A , C , respectively, are the added mass and its Coriolis component matrix. The added mass is calculated based on a 2D panel method, Bertram et al. (2006). Low frequency added mass is used for the horizontal motions (surge, sway and yaw) and the wave frequency added mass is used for the other three modes. The forward speed corrections are added to the wave frequency added mass of heave, roll and pitch based on Salvesen et al. (1970). The wave frequency added mass is a function of the encountering frequency. Therefore, these coefficients are calculated for each time step's corresponding encountering frequency during the simulation. The surge added mass is calculated based on a semi-empirical method proposed by Rajendran et al. (2015a). The Coriolis component matrix of the added mass is given by,

$$C = \begin{bmatrix} 0 & A_{22}r & 0 & A_{24}r & 0 & A_{26}r \\ 0 & 0 & 0 & 0 & 0 & -A_{11}u \\ 0 & 0 & 0 & 0 & 0 & 0 \\ 0 & 0 & 0 & 0 & 0 & 0 \\ 0 & 0 & 0 & 0 & 0 & 0 \\ -A_{22}v & A_{11}u & 0 & 0 & 0 & 0 \end{bmatrix} \quad (4)$$

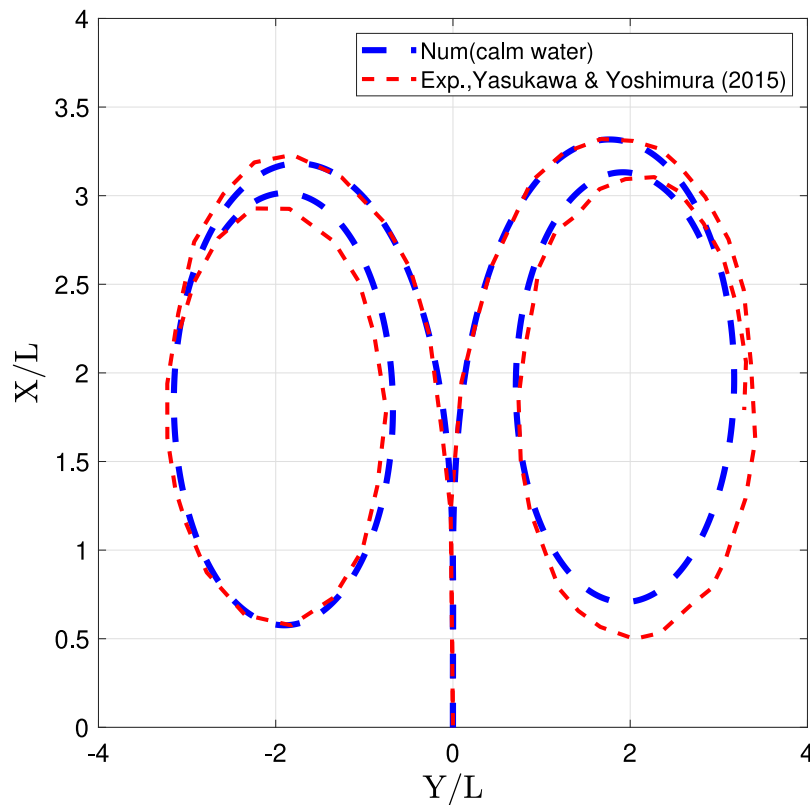


Fig. 3. Open-loop simulation-turning circle in calm water.

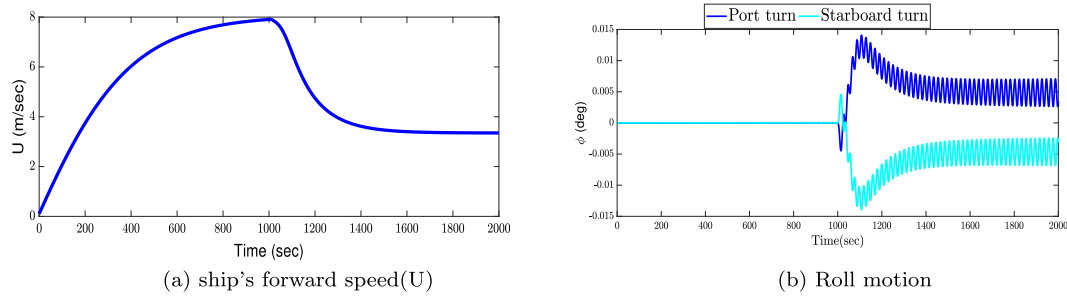


Fig. 4. Time history of ship's forward speed and roll motion obtained from open-loop simulation in calm water.

The wave radiation damping for the vertical motion (heave and pitch) and the associated forward speed correction is calculated based on Salvesen et al. (1970). The damping related to the low-frequency motions is dominated by the viscous effect and are expressed in terms of hydrodynamic derivatives/forces, as shown in the following section. F_P , F_R , F_H are the propeller, rudder and hydrodynamic forces, respectively. F_{FK} , F_D is the Froude-Krylov, diffraction forces and $F_{Secondorderdrift}$ is the mean second order drift force. Velocity vector $v = [u, v, w, p, q, r]$ is defined in body frame and the position vector $\eta = [x, y, z, \phi, \theta, \psi]$ is measured w.r.t global frame. $R(\eta)$ is the Euler angle transformation matrix from the body frame to the inertial frame. It is given by the following matrix,

$$R(\eta) = \begin{bmatrix} c\psi c\theta & -s\psi c\phi + c\psi s\phi s\theta & s\psi s\phi + c\psi c\phi s\theta \\ s\psi c\theta & c\psi c\phi + s\phi s\theta s\psi & -c\psi s\phi + s\theta s\psi c\phi \\ -s\theta & c\theta s\phi & c\theta c\phi \end{bmatrix} \quad (5)$$

where s and c stands for sin and cosine functions respectively.

2.1. Forces/moment

Force due to propeller (F_P) in surge direction is expressed as,

$$F_P = (1 - t_p)T \quad (6)$$

The thrust (T) from the propeller is given by the expression below,

$$T = \rho n_p^2 D_p^4 K_T (J_p) \quad (7)$$

where t_p is the thrust deduction factor, n_p is the propeller speed, D_p is the diameter of the propeller, K_T is the propeller thrust open water characteristic and J_p is the advance coefficient. Force due to rudder in surge, sway and yaw is given by,

$$\begin{aligned} X_R &= -(1 - t_R)F_N \sin \delta \\ Y_R &= -(1 + a_H)F_N \cos \delta \\ N_R &= -(1 + a_H x_H)F_N \cos \delta \end{aligned} \quad (8)$$

where t_R is the steering resistance deduction factor, a_H is the rudder force increase factor, x_H is the longitudinal coordinate of the acting point of the additional lateral force component induced by steering.

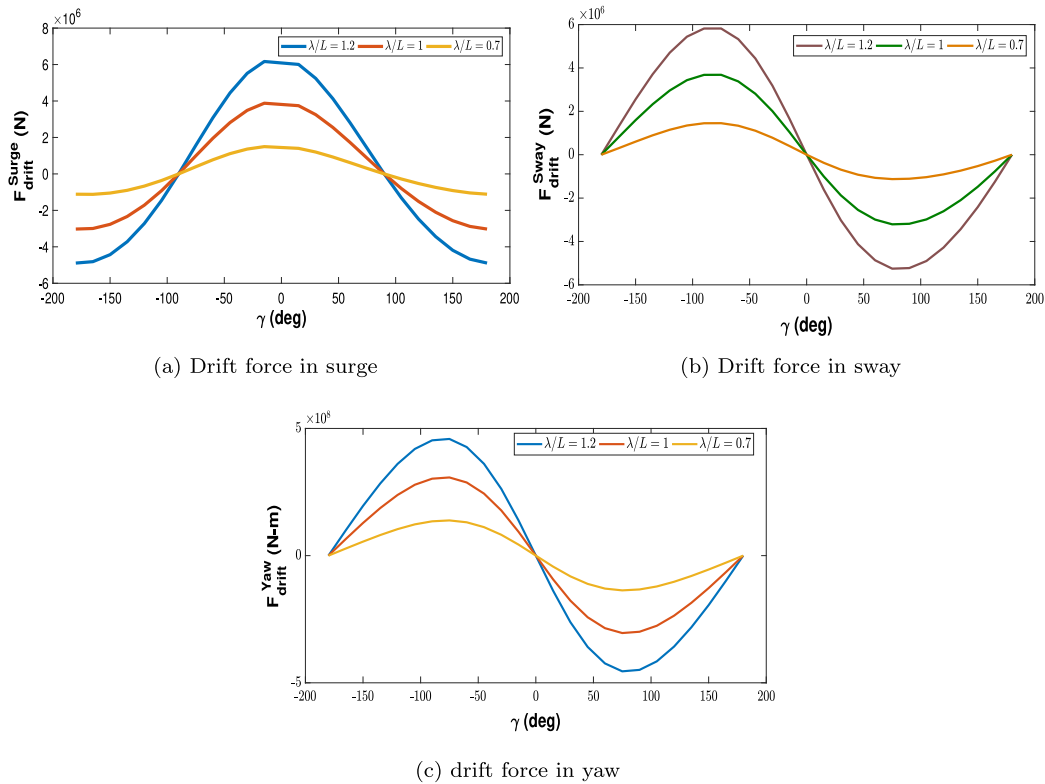


Fig. 5. Mean second-order wave load as a function of wave heading $\gamma \in [-180^\circ, 180^\circ]$.

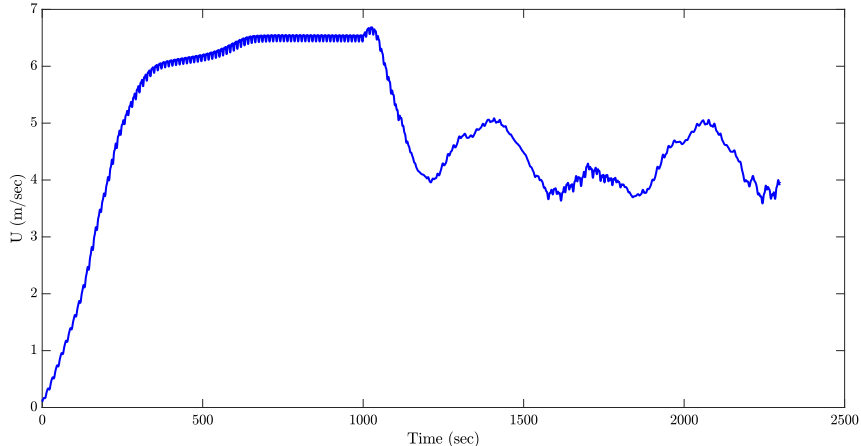


Fig. 6. Ship's forward speed (U) during turning circle simulation in head waves with $\frac{\lambda}{L} = 1$.

Rudder normal force F_N is given by,

$$F_N = 1/2\rho A_R U_R^2 f_\alpha \sin \alpha_R \quad (9)$$

where A_R is the Rudder area, f_α is the rudder lift gradient coefficient, U_R is the resultant of the tangential and normal inflow velocity components of rudder. Tangential component (v_R) of the rudder inflow velocity is given by,

$$v_R = U \gamma_R \beta_R \quad (10)$$

where γ_R and β_R are respectively the flow straightening coefficient and effective inflow angle to the rudder. The normal inflow velocity component (u_R) is expressed as,

$$u_R = u(1 - w_p)(0.446(\sqrt{1 + k \frac{8K_T}{\pi J_p^2}} - 1) + 0.9659) \quad (11)$$

where w_p is the wake coefficient, J_p the propeller advanced ratio. The hydrodynamic force acting on the hull is given by,

$$\begin{aligned} X_H &= -R_0 + X_{vv}v^2 + X_{vr}vr + X_{rr}r^2 + X_{vvvv}v^4 \\ Y_H &= Y_v v + Y_r r + Y_{vv}v^3 + Y_{vr}v^2r + Y_{vr}vr^2 + Y_{rr}r^3 \\ N_H &= N_v v + N_r r + N_{vv}v^3 + N_{v^2}vvr + N_{vr}vr^2 + N_{rr}r^3 \\ K_H &= Y_H(\Delta/2) \end{aligned} \quad (12)$$

where Δ is the draft of the hull. Empirical relations for K_T , w_p , constants representing the interaction between ship hull and the rudder t_R , a_H , x_H and t_p , β_R , γ_R and hydrodynamic derivatives associated in Eq. (12) and ship's resistance coefficient (R_0) are presented in Yasukawa and Yoshimura (2015) for KVLCC2 tanker.

The manoeuvring motions (surge, sway and yaw) are largely affected by the mean second order drift forces. These forces are calculated based on the method proposed by Salvesen (1974). The longitudinal

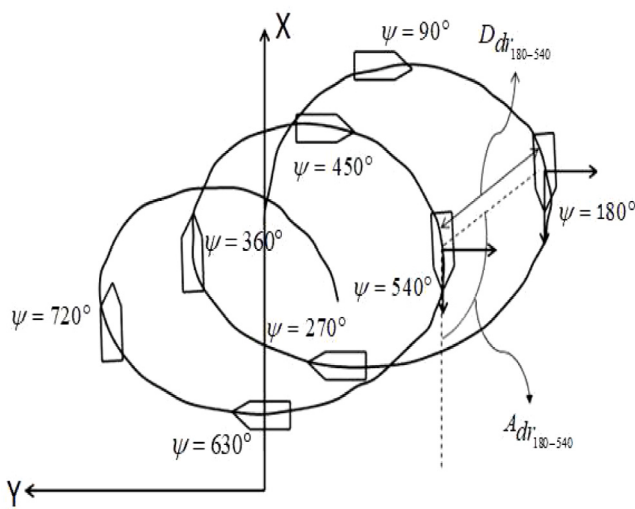


Fig. 7. Pictorial illustration of drifting distance and drifting angle.

and lateral drift forces and the 2nd order yaw moments are pre-calculated for a range of frequency and heading. During the manoeuvring simulations, the encountering wave heading with respect to the ship's x -axis changes. The drift forces/moment are interpolated for the corresponding wave heading for each time step. For heave, roll and pitch, the exciting force on the body due to the action of waves can be resolved into two components, namely, the force due to the incident wave velocity potential and the force due to the diffracted wave velocity potential. The Froude-Krylov forces/moment, due to the incident wave velocity potential, are calculated based on strip theory. The ship is discretized along the length into a finite number of strips. Section curves defining the cross section of each strip are further discretized into finite number of line segments. The surface elevation of the wave is computed using the following expression,

$$\eta = A \cos(-kX \cos \gamma + kY \sin \gamma + \omega t + \epsilon) \quad (13)$$

where A is the wave amplitude, ω is the frequency of the incident wave, k is the wave number, ϵ phase difference.

The Froude-Krylov forces/moment for the exact wetted surface area below the mean water level acting on the line segment of a section is given in Eq. (14),

$$f_j^I(\vec{X}, t) = \rho g A e^{kZ} \cos(-ikX \cos \gamma + ikY \sin \gamma + \omega t + \epsilon) N_j d l \quad (14)$$

where X, Y, Z are the instantaneous position of the midpoint of the line segments in a strip (section) in the inertial frame ($\vec{X} = X\vec{i} + Y\vec{j} + Z\vec{k}$). N_j is the outward normal of the line segments in the inertial frame. Above the mean water level, the pressure is assumed to be hydrostatic. The inertial forces f_j^I are converted into the body frame based on Euler angles R .

$$f_j^B(\vec{x}, t) = R^{-1} f_j^I, j = 1, 2, 3 \quad (15)$$

The Froude-Krylov moments in the body frame are calculated based on following equation,

$$f_k^B(\vec{x}, t) = \vec{r} \times f_j^B, k = 4, 5, 6 \quad (16)$$

where \vec{r} is the position vector of the line segments in each strip. Finally the Froude-Krylov forces/moment in the body frame are calculated for each time instant by integration,

$$F_{j,k}^B(t) = \int_L^{stb} \left(\sum_{port} f_{j,k}^B(\vec{x}, t) \right) dx \quad (17)$$

Similarly, the restoring forces are calculated for the exact wetted surface area for each time step. The instantaneous heave buoyancy

forces acting on each line segment of a section can be calculated as,

$$r_3^I(\vec{X}, t) = \rho g Z N_z d l \quad (18)$$

where Z is the instantaneous Z -coordinate of the centroid of each line segment measured in the inertial frame, dl is the length of the line segment, N_z is the unit normal vector in the Z -direction. In a similar manner to Eqs. (15) and (16), the sectional buoyancy forces in the body frame, r_3^B , are calculated from r_3^I based on Euler angles and the corresponding sectional moments in the body frame are calculated. Finally, they are integrated along the length of the ship to calculate the total buoyancy force. The final restoring forces/moment are calculated based on the difference between the total buoyancy force/moment and the weight/moment due to the weight of the ship. Therefore, the roll and pitch restoring moments can be calculated as

$$R_3^B(t) = \int_L^{stb} \left[\sum_{port} [r_3^B] \right] dx + W_3 \quad (19)$$

$$R_4^B(t) = - \int_L^{stb} \left[\sum_{port} [zr_3^B - yr_3^B] \right] dx - W_2 z_c + W_3 y_c \quad (20)$$

$$R_5^B(t) = - \int_L^{stb} \left[\sum_{port} [xr_3^B] \right] dx - W_3 x_c + W_1 z_c \quad (21)$$

where \vec{W} is the weight vector and its components are resolved in the body frame ($\vec{W} = W_1 \vec{i} + W_2 \vec{j} + W_3 \vec{k}$). It is assumed that the diffraction forces are linear and are calculated based on STF theory (Salvesen et al., 1970). The sectional diffraction forces/moment are integrated over the ship length to get the total force/moment as given by the expressions below,

$$h_j^B(x) = \omega_0 e^{-ikx \cos \gamma} \int_{C_x} (in_3 - n_2 \sin \gamma) e^{iky \sin \gamma} e^{kz} \psi_j d l \quad (22)$$

$$F_{D_j}^B(t) = Re[\rho A e^{i(\omega_e t + \epsilon)} \int_L h_j d x], j = 3, 4 \quad (23)$$

$$F_{D_5}^B(t) = Re[\rho A e^{i(\omega_e t + \epsilon)} \int_L [xh_3 + \frac{U}{i\omega_e} h_3] d x] \quad (24)$$

where ψ_j is the two dimensional velocity potential and are calculated based on 2D panel method, n_2, n_3 are the outward unit normal vectors in y and z directions respectively in body frame, ω_e is the encounter frequency and x is the distance of each strip measured from the body frame. In order to take account of the varying encounter heading angle, the diffraction forces are calculated for a range of heading angles a priori and stored in the database. During the manoeuvring simulations, the diffraction force values from the data base are interpolated to calculate the forces for the corresponding encounter heading angle.

The sectional added mass is calculated based on 2D panel method (Bertram et al., 2006). Zero-frequency added mass is used for the motions in the horizontal and transverse plane and the wave frequency added mass is used for heave and pitch motions. The forward speed correction and the end effects for heave and pitch motion, added mass and damping coefficient are estimated based on STF theory. Because of the change in encountering frequency during simulation, the heave and pitch's added mass values are obtained through interpolation for corresponding encountering frequency.

3. Open-loop simulation

3.1. Numerical setup

The ordinary differential equations, defining the equation of motion in body frame, are solved in the time domain by using Runge-Kutta 4th order method with a constant time step of 0.1 s. The initial conditions of the states are $u = 0.1$ m/s, $v = w = p = q = r = 0$, $\delta = 0$ and $n = 1.75$ rps. To obtain the wave forces, the ship is divided along the length into a number of stations and the cross sections at each

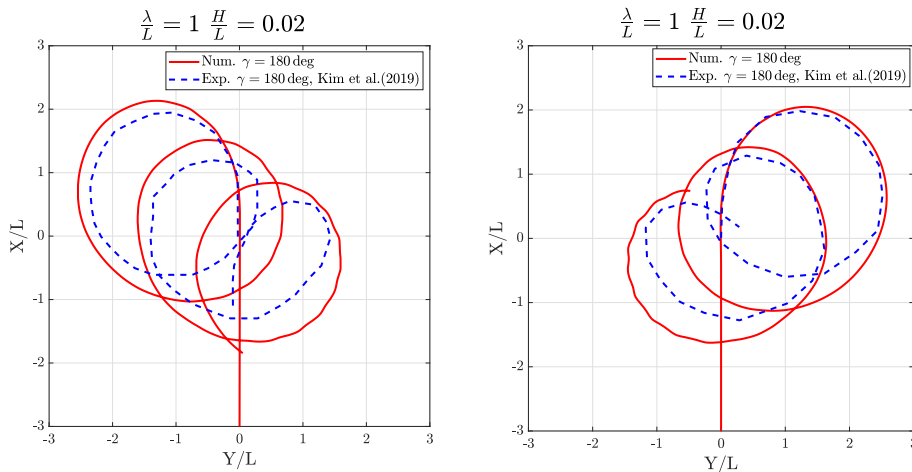


Fig. 8. Comparison of turning circle trajectory in head waves ($\frac{\lambda}{L} = 1$) with the experimental trajectory.

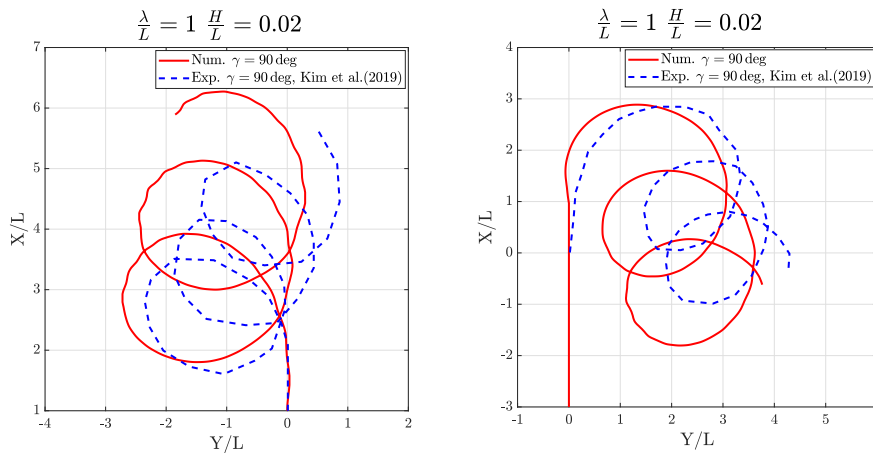


Fig. 9. Comparison of turning circle trajectory in beam waves ($\frac{\lambda}{L} = 1$) with the experimental trajectory.

station is further discretized into a number of segments. In order to identify the spatial and temporal discretization errors, the open-loop simulations are conducted for different number of segments and time step. Each stations are discretized into 20, 40 and 60 segments and each simulations are tested for 3 time steps, i.e., 0.05, 0.1 and 0.15 s. The advance, tactical diameter and transfer are calculated for each discretization and are given in Table 1 and the turning circles for each case are shown in Fig. 2. Table 1 shows that the error is always less than 2% for all combinations of discretization. Therefore, further simulations are carried out with 40 segments per station and 0.1 s time step.

3.2. Calm water

The open-loop simulation is carried out on a KVLCC2 tanker for 35° starboard and port side turn in calm water. The main particulars of KVLCC2 tanker is given in Table 2. The rudder, propeller and the hydrodynamic resistance to the ship hull is modelled as per the MMG model given by Yasukawa and Yoshimura (2015). During the simulation, the ship's steady-state forward speed is set at 15.5 knots, corresponding to a propeller speed of 1.75 rps. The simulation is run using the 6 DoF model. The rudder is activated when the ship reaches the steady forward speed at around 1000 s. The ship's forward and the transfer is compared with the values obtained from free running model tests given by Yasukawa and Yoshimura (2015). The longitudinal rudder inflow velocity component (u_R) is calculated as given in Eq. (11),

$$u_R = 1.2u(1 - w_p)(0.446(\sqrt{1 + k \frac{8K_T}{\pi J_p^2}} - 1) + 0.9659) \quad (25)$$

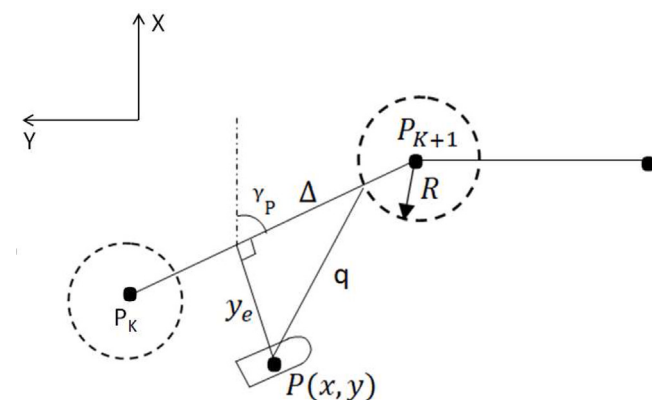


Fig. 10. LOS guidance system.

The turning circle trajectory obtained in the present study with an increased longitudinal rudder inflow velocity u_R (20% increase) is compared with the experimental trajectory and is shown in Fig. 3. The time history of ship's forward speed (U) and roll motion is shown in Fig. 4. The steady-state ship speed is 7.97 m/s. As expected, the ship turns to the port side while taking a starboard turn and vice versa, as shown in Fig. 4.

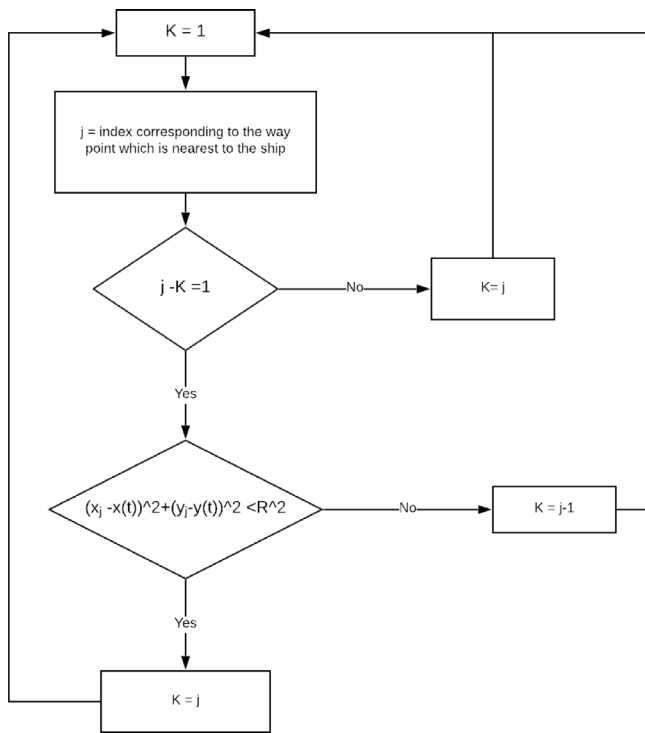


Fig. 11. Way-points selection.

Table 2
Principal particulars of KVLCC2 tanker.

Particular	Full scale
Length between perpendiculars (m)	320
Breadth (m)	58
Draft (m)	20.8
Displacement Δ (m^3)	312600
mass (kg)	3.12×10^8
I_x ($kg \cdot m^2$)	1.43×10^{11}
I_y ($kg \cdot m^2$)	1.99×10^{12}
I_z ($kg \cdot m^2$)	1.99×10^{12}
Longitudinal centre of gravity X_G (m)	11.2
Block coefficient C_b	0.810
Propeller dia. D_p (m)	9.86
Rudder height H_R (m)	15.80
Rudder area A_R (m^2)	112.5

Table 3
Comparison of turning circle parameters with experimental values given by Yasukawa and Yoshimura (2015).

Particulars	Advance	Tactical Dia.	Transfer
Simulation ($\delta = -35$ deg)	3.18	3.11	1.8
Yasukawa and Yoshimura (2015)	3.11	3.08	1.95
Simulation ($\delta = 35$ deg)	3.30	3.17	1.67
Yasukawa and Yoshimura (2015)	3.25	3.34	1.7

Table 3 shows the comparison between the obtained numerical turning circle characteristics and the experimental values. The overall trajectory and the turning circle parameters of the ship matches very closely with the experiments. The largest error is observed for transfer when the vessel takes a port side ($\delta = -35^\circ$) turn and is found to be 7.69%.

3.3. Simulation in waves

Before integrating the controller into the manoeuvring model, the accuracy of the wave force modelling is estimated by comparing the

open loop turning circle simulation results in waves with the experimental results. The behaviour of the KVLCC2 tanker is predicted in regular waves using the model given by Eq. (1). The simulation is carried out in head and beam waves with a frequency of 0.44 rad/s corresponding to a wave to ship length ratio ($\frac{H}{L}$) of 1 and a wave steepness ($\frac{H}{\lambda}$) of 0.02. The propeller speed is kept constant at 1.75 rps. The Froude number (F_n) chosen for the simulation is 0.142, which corresponds to a ship's forward speed of 15.5 knots in calm water. Fig. 5 shows the mean second order wave drift force in surge, sway and yaw obtained for different wave conditions (i.e., $\frac{H}{L} = 0.7, 1, 1.2$) and for different wave headings between -180° to 180° using Salvesen method. It is understood that Salvesen method is not applicable for shorter waves. Therefore, we have limited our study to longer waves with a wave to ship length ratio of 0.7 and higher. Fig. 6 shows the time history of the ship's forward speed during the simulation. For the propeller rpm same as the calm water condition, a 25% reduction in the ship's speed is observed. This is due to the added resistance in head seas. The simulation is run for 2500 s and the rudder is activated at 1000 s at which the ship attains the steady-state speed. The ship is in the acceleration phase up to 1000 s and the rudder is activated at this moment. There is a 30% reduction in the ship's forward speed when the rudder is activated.

Generally ship's turning trajectories in waves are studied in terms of second advance with a heading of 450° and second tactical diameter with a heading of 540° (Yun et al., 2015), in addition to traditional advance and tactical diameter. In the present study, the trajectory is analysed in terms of drifting distances and drift angles. The drifting distance, for example, $Ddr_{180-540}$ is obtained by measuring the length of the line drawn between two points, which corresponds to the ship heading angles of 180° and 540° , as represented in Fig. 7. Drifting angle $Adr_{180-540}$ is the angle between the ship's initial approach direction and the line drawn.

The trajectory obtained from the simulation in head waves is shown in Fig. 8 and in beam waves in Fig. 9. The trajectory is compared with the experimental trajectory. The comparison of the drifting distance obtained in head and beam waves is presented in Table 4 and drifting angles in Table 5. The autopilot model is tested in head waves. For the open-loop head wave case ($\chi = 180^\circ$), when the ship is turning starboard ($\delta = +35^\circ$), the largest error occurs for Ddr_{90-450} . However, for all other drifting distances in head waves, the numerical model can predict the drifting distance within 10% error. Similarly, when the ship is turning port side ($\delta = -35^\circ$), the largest error (25%) occurs for $Ddr_{270-630}$. Drifting angles are better predicted than the drifting distances. In head waves, the largest error in the estimation of the drifting distance and drifting angles are 28% and 11%, respectively and these occur when the ship is in beam sea condition. As we can notice in Figs. 8 and 9, using the model given in Eq. (1), the predicted behaviour of the ship in waves is in fairly good agreement with the experimental behaviour as given by Kim et al. (2019).

4. LOS guidance

The desired trajectory is assumed to be straight lines joining the way-points P_K and P_{K+1} , where, the subscript $K = 1, 2, \dots, n-1$ indicates the index of the way-point and n is the number of way-points. The desired heading angle $\psi_d(t)$ is computed based on the ship's position $P(x, y)$ and the deviation of the ship (y_e) from the desired path at any given instant of time as represented in Fig. 10. By choosing a constant look ahead distance (q), the desired heading angle is computed by using the expressions below (Lekkas and Fossen, 2013),

$$\psi_d(t) = \gamma_P + \text{atan}\left(\frac{-y_e(t)}{\Delta}\right) - \text{atan}\left(\frac{v}{u}\right) \quad (26)$$

where $\gamma_P = \text{atan}2(yd_{K+1} - yd_K, xd_{K+1} - xd_K)$, $\Delta = \sqrt{(q^2 - (y_e)^2)}$. The deviation of the ship from the desired trajectory is computed by using the expression below,

$$y_e(t) = -(x(t) - xd_K) \sin \gamma_P + (y(t) - yd_K) \cos \gamma_P \quad (27)$$

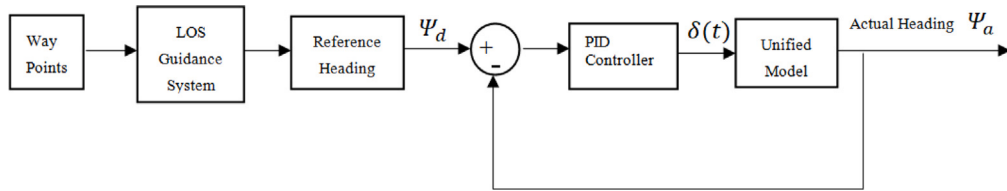
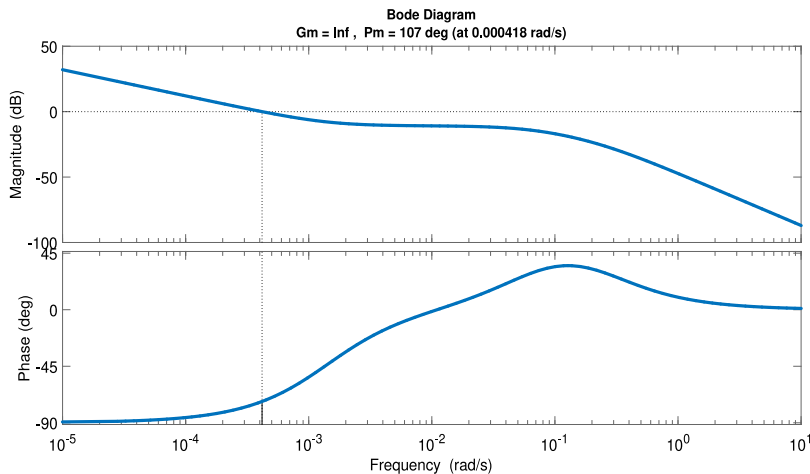
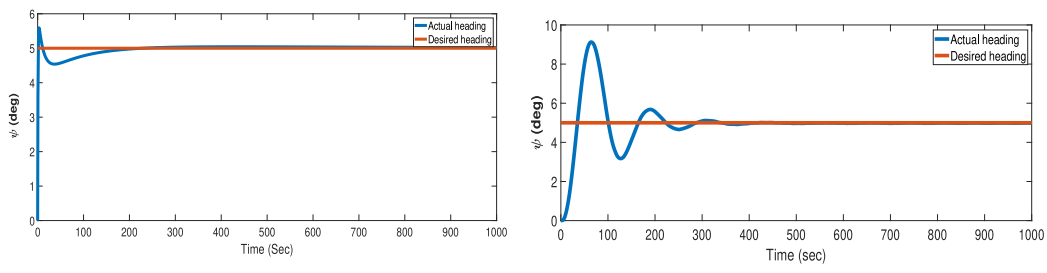
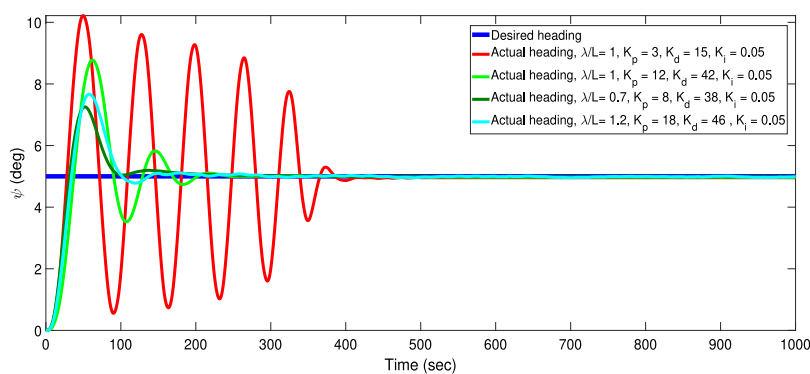
**Fig. 12.** Schematic representation of closed-loop system for heading control.**Fig. 13.** Frequency analysis using Bode plot. Gm — Gain margin, Pm — Phase margin.**Fig. 14.** System response in calm water for 5° step desired heading angle.**Fig. 15.** Unified model response in waves for 5° step desired angle.

Table 4
Comparison of drifting distance in head and beam waves with experimental values.

Particulars	δ (deg)	χ (deg)	H/L	λ/L	Ddr_{90-450}	$Ddr_{180-540}$	$Ddr_{270-630}$	$Ddr_{360-720}$
Simulation	+35	180	0.02	1	1.25	1.18	1.19	1.11
Kim et al. (2019)					0.97	1.11	1.10	1.16
Simulation	+35	90	0.02	1	1.44	1.37	1.47	1.51
Kim et al. (2019)					1.28	1.06	1.06	1.33
Simulation	-35	180	0.02	1	1.17	1.06	1.42	1.07
Kim et al. (2019)					0.96	1.13	1.14	1.27
Simulation	-35	90	0.02	1	1.22	1.44	1.27	1.12
Kim et al. (2019)					0.66	0.86	0.91	0.88

Table 5
Comparison of drift angle in head and beam waves with experimental values.

Particulars	δ (deg)	η (deg)	H/L	λ/L	Adr_{90-450}	$Adr_{180-540}$	$Adr_{270-630}$	$Adr_{360-720}$
Simulation	+35	180	0.02	1	120	128	115	135
Kim et al. (2019)					135	125	128	129
Simulation	+35	90	0.02	1	206	203	203	197
Kim et al. (2019)					216	207	215	218
Simulation	-35	180	0.02	1	237	243	243	239
Kim et al. (2019)					222	234	233	242
Simulation	-35	90	0.02	1	352	348	341	348
Kim et al. (2019)					332	323	328	329

where xd_K , yd_K are the coordinates of the way-points measured w.r.t earth-fixed frame and the subscript K indicates the index of the way point, which is chosen based on the condition, $(xd_K - x(t))^2 + (yd_K - y(t))^2 < R^2$ and it is illustrated in Fig. 11. R is chosen to be 1.5 times the ship length and look ahead distance(q) is fixed at twice the ship length. The ship initially starts from the first way-point and hence $K = 1$ in Fig. 11.

5. Closed-loop simulation with waves

A PID controller as shown in Fig. 12 is integrated with the unified 6 DoF model. The environmental disturbance to the ship mainly comes from the wave force. These forces are modelled using strip theory and included in the system dynamics as given in Eq. (1). Input to the controller is the desired heading angle, which is obtained from a Line of Sight (LoS) algorithm and the actual heading of the ship. The output from the controller is the control signal to actuate the rudder. The saturation rudder angle limit $-35^\circ \leq \delta(t) \leq 35^\circ$ and rate limit $\dot{\delta}(t) \leq 2.34^\circ/\text{s}$ is included in the model. The simulation is run in head sea condition for different wave to ship length ratios ($\frac{\lambda}{L} = 0.7, 1, 1.2$) in order to emulate the actual sea. During the simulations, the wave steepness is kept constant at 0.02($\frac{H}{\lambda} = 0.02$).

The frequency of the incident wave is 0.44 rad/s corresponding to wave to ship length ratio of $\frac{\lambda}{L} = 1$. The control law used in the controller design is given by,

$$\delta(t) = K_p(\psi_d - \psi_a(t)) + K_d r + K_i \int_0^t (\psi_d - \psi_a(t)) dt \quad (28)$$

where K_p , K_d and K_i are proportional, derivative and integral gains of PID controller respectively.

5.1. PID gains

The external load changes with wave conditions. Hence the controller gains need to be adjusted to changing external loads. Generally

Table 7
PID Controller gains used for different sea conditions.

$\frac{\lambda}{L}$	Frequency (rad/s)	Amplitude (m)	K_p	K_d	K_i
Calm water	0	0	5	12	0.05
0.7	0.52	2.24	8	38	0.05
1	0.44	3.2	12	42	0.05
1.2	0.4	3.84	18	46	0.05

for ships, 6 DoF equation of motion can be divided into 2 sets of coupled equations. First one consists of surge, heave and pitch and the other consists of sway, roll and yaw. Initial PID gains are obtained by considering 2 DoF (sway, yaw) Davidson and Schiff (1946) model. The transfer function relating the ship's actual heading angle (ψ_a) and the rudder angle (δ) is obtained from this model for KVLCC2 tanker and is expressed as below,

$$\frac{\psi_a(s)}{\delta(s)} = \frac{0.0004 + 0.2871s}{64s^3 - 11.53s^2 + s} \quad (29)$$

The frequency analysis is performed to find the gain range within which the system will be stable. The Bode plot is shown in Fig. 13. The gain margin (Gm) of the system is infinity which indicates that the system will be stable for any gain. Similarly, the positive phase margin (Pm) in Fig. 13 indicates that the system is stable. The controller transfer function is given by the following expression,

$$C(s) = K_p(1 + T_d s + \frac{1}{T_i s}) \quad (30)$$

where $T_d = \frac{K_d}{K_p}$ and $T_i = \frac{K_i}{K_p}$. The initial gains, $K_p = 27$, $K_d = 379$, $K_i = 0.3$, were obtained by Ziegler Nichols method (Ogata, 2010) using 2 DoF model for calm water condition. Fig. 14(b) shows the 2 DoF model closed-loop response to achieve a constant heading of 5°. The system reaches the desired heading with a rise time of 950 ms and a maximum overshoot 11.9%. Gains for 6 DoF model are obtained from the initial gains obtained by using 2 DoF model by trial and

Table 6
6 DoF unified model response parameters.

Particulars	$\frac{\lambda}{L}$	Rise time, t_r (s)	Maximum overshoot, M_p (%)	Settling time, t_s (s)
$K_p = 3, K_d = 15, K_i = 0.05$	Calm water	35.3	80	400
$K_p = 3, K_d = 15, K_i = 0.05$	1	28.1	104.2	432.4
$K_p = 12, K_d = 42, K_i = 0.05$	1	37.3	75.34	250.4
$K_p = 8, K_d = 38, K_i = 0.05$	0.7	32	45	215.7
$K_p = 18, K_d = 46, K_i = 0.05$	1.2	34	53	221

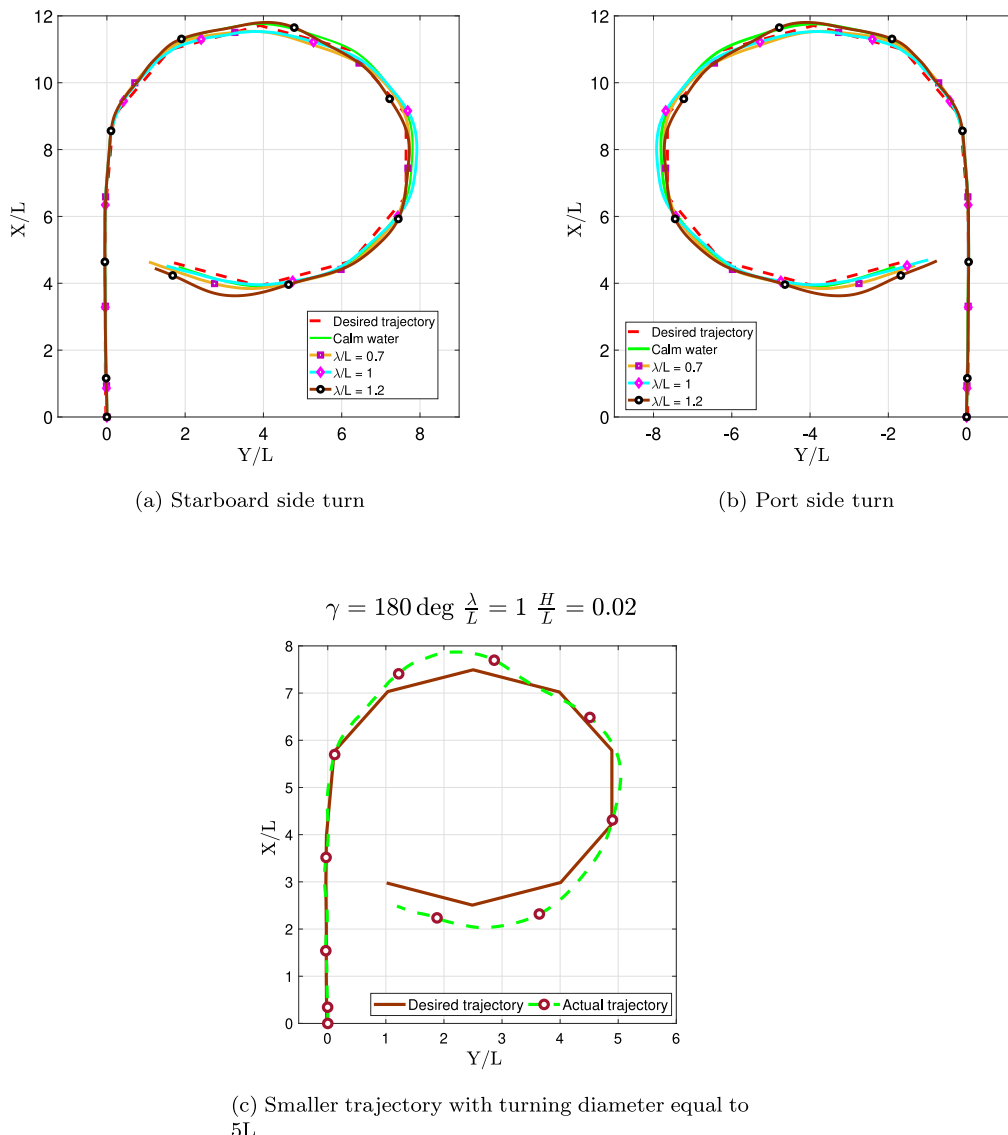
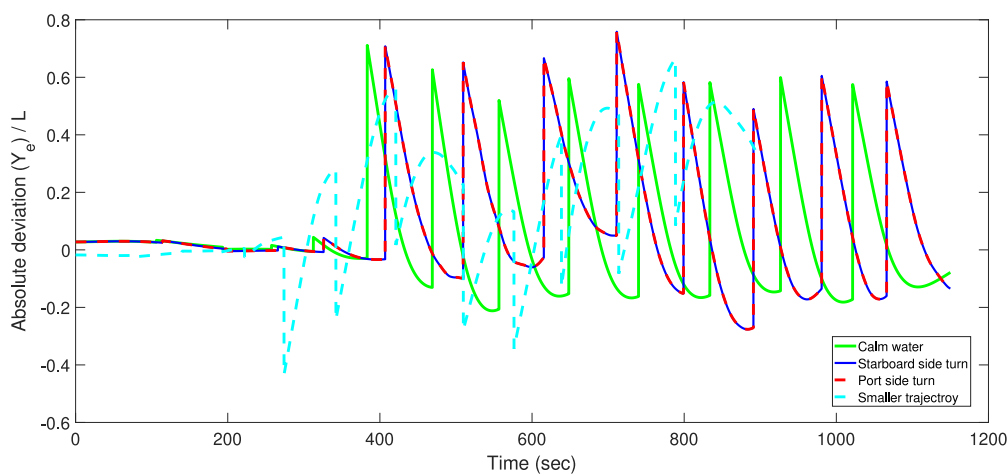


Fig. 16. Path following of KVLCC2 tanker in regular waves using PID controller.

Fig. 17. Time history of absolute deviation of the ship from desired trajectory during path following in waves with $\gamma = 180^\circ$, $\frac{\lambda}{L} = 1$, $\frac{H}{L} = 0.02$. $(Y_e/L)_{max} = 0.78L$ for port and starboard side turn, $(Y_e/L)_{max} = 0.7L$ in calm water, $(Y_e/L)_{max} = 0.66L$ for smaller desired trajectory.

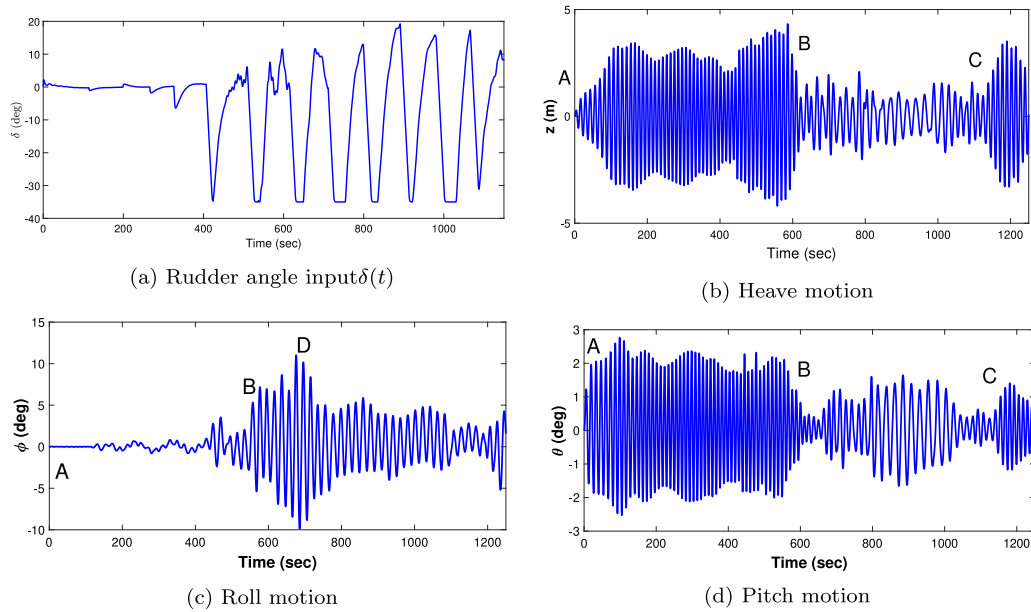


Fig. 18. Time history of rudder angle input and motions during path following corresponding to $\gamma = 180^\circ$, $\frac{\lambda}{L} = 1$, $\frac{H}{L} = 0.02$ wave case.

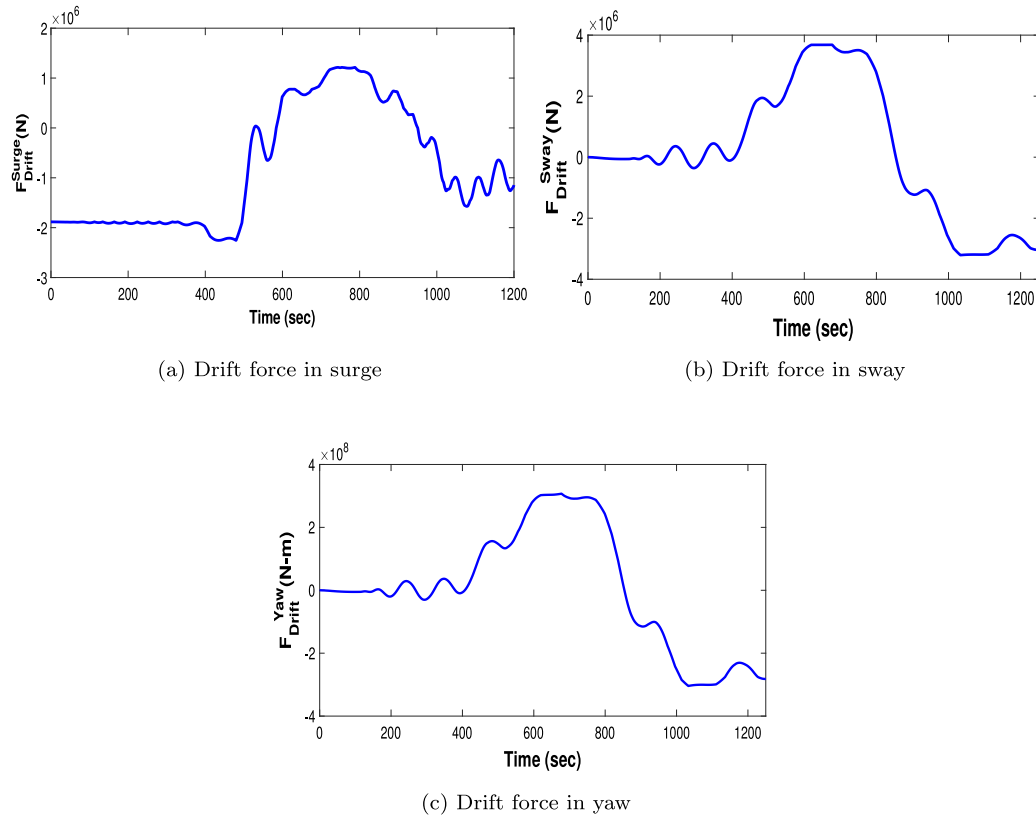


Fig. 19. Time history of mean 2nd order wave load during path following in waves with $\gamma = 180^\circ$, $\frac{\lambda}{L} = 1$, $\frac{H}{L} = 0.02$.

Table 8
Way-points table.

$xd(m)$	0	500	1000	1500	2000	2875	3500	3750	3500	2875	2125	1500	1250	1500
$yd(m)$	0	0	0	0	0	50	500	1250	2000	2500	2500	2000	1250	500

error. The gains are finalized based on the rise time (t_s), overshoot (M_p) and settling time (t_s). Closed-loop system response using 6 DoF model is shown in Fig. 14(a) for step desired heading angle with

$K_p = 3$, $K_d = 15$, $K_i = 0.05$. The unified model response in waves with $\frac{\lambda}{L} = 1$ is shown in Fig. 15. For the same PID gains as in calm water, there are initial oscillations in the response and it take more

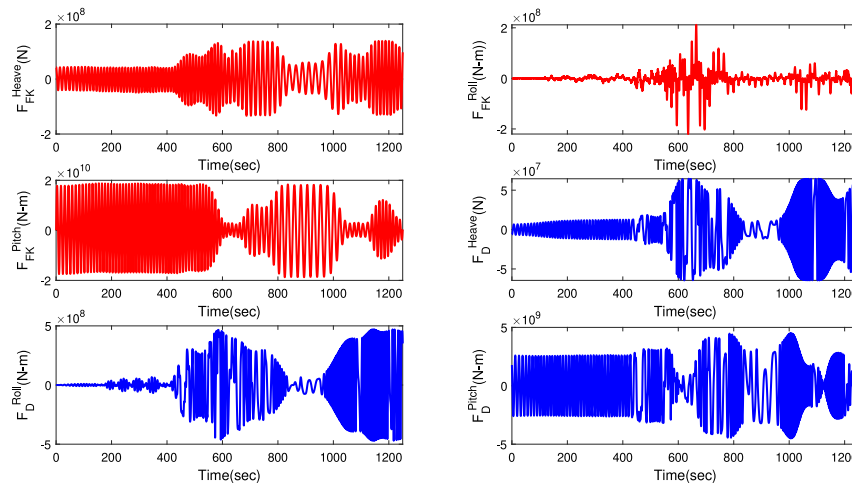


Fig. 20. Froude–Krylov and diffraction forces/moment in heave, roll and pitch obtained from port side path following simulation in waves with $\gamma = 180^\circ$, $\frac{\lambda}{L} = 1$, $\frac{H}{L} = 0.02$.

time to converge to the desired heading angle. To avoid oscillations and reduce settling time, PID gains are further tuned and better response obtained for $K_p = 12$, $K_d = 42$, $K_i = 0.05$. The performance parameters (t_r , M_p , t_s) are tabulated in Table 6 for calm water and in waves for gains discussed here. Similarly for other wave conditions with the wave to ship length ratio 0.7 and 1.2, appropriate gains are chosen based on these parameters and are presented in Table 7.

5.2. Results and discussion on closed loop simulations

The ship is initially at the origin (0, 0) and the propeller speed is fixed at 1.75 rps throughout the simulation. The points given in Table 8 are the X , Y coordinates of the desired locations. The desired trajectory is the line passing through these points and it is chosen such that the turning diameter is at least five times the ship length. Closed-loop simulation result for path following using PID controller is shown in Fig. 16a, 16b for starboard and port side turn in calm water and in different wave conditions i.e., waves with different wave to ship length ratio ($\frac{\lambda}{L} = 0.7, 1, 1.2$) and constant wave steepness $\frac{H}{L} = 0.02$. The path following ability for smaller desired trajectory (i.e., diameter of the trajectory chosen is 5 times the ship length) in waves with $\frac{\lambda}{L} = 1$ is shown in Fig. 16c. Absolute deviation of the ship from the desired trajectory is shown in Fig. 17 for port side turn in calm water, waves with $\frac{\lambda}{L} = 1$ and tighter desired trajectory. Figs. 18a and 18b, 18c, 18d shows the time history of rudder angle input and motions in heave, roll and pitch during port side turn in head waves with a wave to ship length ratio $\frac{\lambda}{L} = 1$. The mean second order drift force in surge, sway and yaw and first order wave excitation force in heave, roll and pitch acting on the ship during this simulation is shown in Figs. 19 and 20, respectively. We can see from Fig. 18a that at any instant of time, rudder angle input given to the system is not exceeding the maximum rudder angle limit constraint considered (i.e., 35 deg on either side of the ship). Absolute deviation (Y_e) of the ship from the desired trajectory is at a maximum of 0.78L for port side turn and starboard side turn. This deviation is mainly due to the large drift force in sway and yaw at 750th second as we can see in Fig. 19b and 19c and the rudder's inability to generate enough turning moment due to the rudder angle saturation limit. Absolute deviation in calm water is approximately 0.7 times the ship length and for tighter trajectory, it is 0.66 times the ship length when $\frac{\lambda}{l} = 1$.

The region marked between A and B in Fig. 18b represents the duration during which the ship is in head waves. During this period, ship will encounter the waves more frequently and hence the frequency of heave motion during this period is high. Between B–C, the ship is in oblique sea condition and the frequency of heave motion is relatively

less as compared to the frequency between A–B. Similar behaviour can be observed in roll and pitch motions as well in Fig. 18c and 18d. The magnitude of heave and pitch motions between A–B is relatively high compared to the magnitude between B–C. In Fig. 18c, between A–B the roll motion is negligible. This is due to the symmetry of the hull w.r.t longitudinal plane of the hull and the ship is in head waves. The roll motion slowly starts increasing in the oblique wave and it is maximum at D where the ship is in beam sea condition. The maximum roll motion magnitude is approximately 12 deg and it occurs at around 700 s. From these observations it is clear that the motions obtained from the simulation is realistic in nature.

6. Conclusion

A unified seakeeping and manoeuvring model for predicting ship manoeuvring in waves is used for PID controller design for heading control. The 2nd order mean drift forces are calculated based on Salvesen method and affect the motions in the horizontal plane. The roll, heave and pitch motions are affected by the first order wave excitation forces. The body non-linear Froude–Krylov and restoring forces are calculated for the exact wetted surface. Numerical open-loop manoeuvring simulations are carried out in calm water and in waves with wave length equal to ship length. The numerical results are in fairly good agreement with the experimental results. The unified model is further integrated with a PID controller and its effectiveness is studied.

The controller gains K_p , K_d and K_i are obtained for KVLCC2 tanker for different sea states and the controller performance is studied numerically by navigating the ship through a set of pre-defined way-points using LOS algorithm. The largest cross track error of 0.78L is observed for port and starboard turn. This deviation is mainly due to the large drift force in sway and yaw when the ship is in oblique sea condition. The numerical model can be used to estimate the control gains in different sea states and the corresponding cross track error a priori and hence will be useful in generating a controller gain data bank.

Declaration of competing interest

The authors declare that they have no known competing financial interests or personal relationships that could have appeared to influence the work reported in this paper.

Acknowledgements

This project is funded by the Science and Engineering Research Board (SERB) under the project no: CRG/2018/004807. The authors are indebted to Prof. Antonio Pascoal, Instituto Superior Technico (IST), Portugal and Dr. Ranjith Mohan, IIT Madras, India for providing insights into the control system design (SPARC Project No: SPARC/2018-2019/P935/SL).

References

- Bailey, P., 1997. A unified mathematical model describing the maneuvering of a ship travelling in a seaway. *Trans. RINA* 140, 131–149.
- Bertram, V., 2011. Practical Ship Hydrodynamics. Elsevier.
- Bertram, V., Söding, H., Graf, K., Croisic, L., 2006. PDSTRIP—a strip method for ship and yacht seakeeping. In: Numerical Towing Tank Symposium, vol. 8, pp. 19–22.
- Do, K.D., Jiang, Z.-P., Pan, J., 2002. Underactuated ship global tracking under relaxed conditions. *IEEE Trans. Automat. Control* 47 (9), 1529–1536.
- Duclos, G., Clément, A.H., Chatry, G., et al., 2001. Absorption of outgoing waves in a numerical wave tank using a self-adaptive boundary condition. *Int. J. Offshore Polar Eng.* 11 (03).
- Encarnacao, P., Pascoal, A., 2000. 3D path following for autonomous underwater vehicle. In: Proceedings of the 39th IEEE Conference on Decision and Control (Cat. No. 00CH37187), vol. 3, IEEE, pp. 2977–2982.
- Fang, M.-C., Luo, J.-H., Lee, M.-L., 2005. A nonlinear mathematical model for ship turning circle simulation in waves. *J. Ship Res.* 49 (2), 69–79.
- Fonseca, N., 1998. Nonlinear wave-induced responses of ships in irregular seas. In: Proceedings of the 12th International Conference on Offshore Mechanics and Arctic Engineering, OMAE'98. ASME.
- Fonseca, N., Guedes Soares, C., 1998. Time-domain analysis of large-amplitude vertical ship motions and wave loads. *J. Ship Res.* 42 (2), 139–152.
- Fossen, T.I., 2005. A nonlinear unified state-space model for ship maneuvering and control in a seaway. *Int. J. Bifurcation Chaos* 15 (09), 2717–2746.
- Fossen, T.I., Breivik, M., Skjetne, R., 2003. Line-of-sight path following of underactuated marine craft. *IFAC Proc. Vol.* 36 (21), 211–216.
- Fossen, T.I., Pettersen, K.Y., Galeazzi, R., 2014. Line-of-sight path following for dubins paths with adaptive sideslip compensation of drift forces. *IEEE Trans. Control Syst. Technol.* 23 (2), 820–827.
- Guerreiro, B.J., Silvestre, C., Cunha, R., Pascoal, A., 2014. Trajectory tracking nonlinear model predictive control for autonomous surface craft. *IEEE Trans. Control Syst. Technol.* 22 (6), 2160–2175.
- Jefferys, E., 1984. Simulation of wave power devices. *Appl. Ocean Res.* 6 (1), 31–39.
- Jiang, Z.-P., Nijmeijer, H., 1999. A recursive technique for tracking control of nonholonomic systems in chained form. *IEEE Trans. Automat. Control* 44 (2), 265–279.
- Kim, D.J., Yun, K., Park, J.-Y., Yeo, D.J., Kim, Y.G., 2019. Experimental investigation on turning characteristics of KVLCC2 tanker in regular waves. *Ocean Eng.* 175, 197–206.
- Lee, G., Surendran, S., Kim, S.-H., 2009. Algorithms to control the moving ship during harbour entry. *Appl. Math. Model.* 33 (5), 2474–2490.
- Lekkas, A.M., Fossen, T.I., 2013. Line-of-sight guidance for path following of marine vehicles. *Adv. Mar. Robot.* 63–92.
- Moradi, M., Katebi, M., 2001. Predictive PID control for ship autopilot design. *IFAC Proc. Vol.* 34 (7), 375–380.
- Moreira, L., Soares, C.G., 2011. Autonomous ship model to perform manoeuvring tests. *J. Marit. Res.* 8 (2), 29–46.
- Ogata, K., 2010. Modern Control Engineering. Prentice hall.
- Oh, S.-R., Sun, J., 2010. Path following of underactuated marine surface vessels using line-of-sight based model predictive control. *Ocean Eng.* 37 (2–3), 289–295.
- Ottosson, P., Bystrom, L., 1991. Simulation of the dynamics of a ship maneuvering in waves. *Trans. Soc. Nav. Archit. Mar. Eng.* 99, 281–298.
- Paul, J., 1998. Modelling of General Electromagnetic Material Properties in TLM (Ph.D. thesis). University of Nottingham.
- Perera, L., Moreira, L., Santos, F., Ferrari, V., Sutulo, S., Soares, C.G., 2012. A navigation and control platform for real-time manoeuvring of autonomous ship models. *IFAC Proc. Vol.* 45 (27), 465–470.
- Peric, M., Bertram, V., 2011. Trends in industry applications of computational fluid dynamics for maritime flows. *J. Ship Prod. Des.* 27 (4), 194–201.
- Pettersen, K., Nijmeijer, H., 1998. Tracking control of an underactuated surface vessel. In: Proceedings of the 37th IEEE Conference on Decision and Control (Cat. No. 98CH36171), vol. 4, IEEE, pp. 4561–4566.
- Rajendran, S., Fonseca, N., Soares, C.G., 2015a. Effect of surge motion on the vertical responses of ships in waves. *Ocean Eng.* 96, 125–138.
- Rajendran, S., Fonseca, N., Soares, C.G., 2015b. Simplified body nonlinear time domain calculation of vertical ship motions and wave loads in large amplitude waves. *Ocean Eng.* 107, 157–177.
- Rajendran, S., Fonseca, N., Soares, C.G., 2016. Body nonlinear time domain calculation of vertical ship responses in extreme seas accounting for 2nd order Froude-Krylov pressure. *Appl. Ocean Res.* 54, 39–52.
- Salvesen, N., 1974. Second-order steady-state forces and moments on surface ships in oblique regular waves. In: Int Symp. on the Dynamics of Marine Vehicles and Structures in Waves.
- Salvesen, N., Tuck, E., Faltinsen, O., 1970. Ship motions and sea loads.
- Seo, M.-G., Kim, Y., 2011. Numerical analysis on ship maneuvering coupled with ship motion in waves. *Ocean Eng.* 38 (17–18), 1934–1945.
- Sira-Ramirez, H., 1999. On the control of the underactuated ship: A trajectory planning approach. In: Proceedings of the 38th IEEE Conference on Decision and Control (Cat. No. 99CH36304), vol. 3, IEEE, pp. 2192–2197.
- Skejic, R., Faltinsen, O.M., 2008. A unified seakeeping and maneuvering analysis of ships in regular waves. *J. Mar. Sci. Technol.* 13 (4), 371–394.
- Skjetne, R., Smogeli, Ø.N., Fossen, T.I., 2004. A nonlinear ship manoeuvring model: Identification and adaptive control with experiments for model ship.
- Son, K., Nomoto, K., 1981. On the coupled motion of steering and rolling of a high speed container ship. *J. Soc. Nav. Archit. Jpn.* 1981 (150), 232–244.
- Sutulo, S., Guedes Soares, C., 2008. A generalized strip theory for curvilinear motion in waves. In: International Conference on Offshore Mechanics and Arctic Engineering, vol. 48234, pp. 359–368.
- Sutulo, S., Soares, C.G., 2019. On the application of empiric methods for prediction of ship manoeuvring properties and associated uncertainties. *Ocean Eng.* 186, 106111.
- Tomera, M., 2017. Fuzzy self-tuning PID controller for a ship autopilot. In: Proceedings of the 12th International Conference on Marine Navigation and Safety of Sea Transportation.
- Tran, N.D., 2014. Line-of-Sight-Based Maneuvering Control Design, Implementation, and Experimental Testing for the Model Ship C/S Enterprise I (Master's thesis). Institutt for marin teknikk.
- Wang, J., Zou, Z., Wang, T., 2018. Path following of a surface ship sailing in restricted waters under wind effect using robust h guaranteed cost control. *Int. J. Nav. Archit. Ocean Eng.*
- Xiang, X., Faltinsen, O.M., 2011. Maneuvering of two interacting ships in calm water. *Mar. Syst. Ocean Technol.* 6 (2), 65–73.
- Xu, H., Oliveira, P., Soares, C.G., 2020. L1 adaptive backstepping control for path-following of underactuated marine surface ships. *Eur. J. Control.*
- Yasukawa, H., Nakayama, Y., 2009. 6-DOF motion simulations of a turning ship in regular waves. In: Proceedings of the International Conference on Marine Simulation and Ship Manoeuvrability. pp. 508–517.
- Yasukawa, H., Yoshimura, Y., 2015. Introduction of MMG standard method for ship maneuvering predictions. *J. Mar. Sci. Technol.* 20 (1), 37–52.
- Yen, T., Zhang, S., Weems, K., Lin, W., 2010. Development and validation of numerical simulations for ship maneuvering in calm water and in waves. In: Proceedings of the 28th Symposium on Naval Hydrodynamics. California, USA. pp. 12–27.
- Yoshimura, Y., 2001. In: Kijima, K. (Ed.), Investigation into the Yaw-Checking Ability in Ship Manoeuvrability Standard. Citeseer.
- Yun, K., Yeo, D., Ryu, G., Lee, Y., 2015. Experimental study on manoeuvrability of KVLCC2 in shallow water by free running model test. In: 13th International Conference on Ship Manoeuvrability and Maritime Simulation. Newcastle, UK.
- Zheng, H., Negenborn, R.R., Lodewijks, G., 2014. Trajectory tracking of autonomous vessels using model predictive control. *IFAC Proc. Vol.* 47 (3), 8812–8818.